AIP | Applied Physics Letters

Phase contrast and operation regimes in multifrequency atomic force microscopy

Sergio Santos

Citation: Applied Physics Letters **104**, 143109 (2014); doi: 10.1063/1.4870998
View online: http://dx.doi.org/10.1063/1.4870998
View Table of Contents: http://scitation.aip.org/content/aip/journal/apl/104/14?ver=pdfcov
Published by the AIP Publishing

Articles you may be interested in

Renormalization, resonance bifurcation, and phase contrast in dynamic atomic force microscopy
J. Appl. Phys. **110**, 094314 (2011); 10.1063/1.3660745

Phase image contrast mechanism in intermittent contact atomic force microscopy
J. Appl. Phys. **108**, 094311 (2010); 10.1063/1.3503478

Triple-frequency intermittent contact atomic force microscopy characterization: Simultaneous topographical, phase, and frequency shift contrast in ambient air
J. Appl. Phys. **108**, 054901 (2010); 10.1063/1.3475644

Multiple impact regimes in liquid environment dynamic atomic force microscopy
Appl. Phys. Lett. **93**, 093111 (2008); 10.1063/1.2976438

Multifrequency, repulsive-mode amplitude-modulated atomic force microscopy
Appl. Phys. Lett. **89**, 113121 (2006); 10.1063/1.2345593

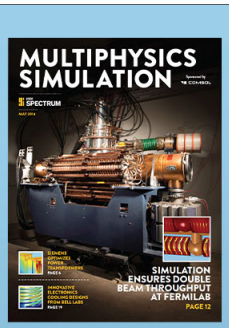

Free online magazine
MULTIPHYSICS SIMULATION
READ NOW
COMSOL

This article is copyrighted as indicated in the article. Reuse of AIP content is subject to the terms at: http://scitation.aip.org/termsconditions. Downloaded to IP: 147.83.121.58 On: Fri, 06 Jun 2014 14:56:29

Phase contrast and operation regimes in multifrequency atomic force microscopy

Sergio Santos
Departament de Disseny i Programació de Sistemes Electrònics, UPC—Universitat Politècnica de Catalunya Av. Bases, 61, 08242 Manresa (Barcelona), Spain

(Received 8 March 2014; accepted 30 March 2014; published online 8 April 2014)

In amplitude modulation atomic force microscopy the attractive and the repulsive force regimes induce phase shifts above and below 90°, respectively. In the more recent multifrequency approach, however, multiple operation regimes have been reported and the theory should be revisited. Here, a theory of phase contrast in multifrequency atomic force microscopy is developed and discussed in terms of energy transfer between modes, energy dissipation and the kinetic energy and energy transfer associated with externally driven harmonics. The single frequency virial that controls the phase shift might undergo transitions in sign while the average force (modal virial) remains positive (negative). © *2014 AIP Publishing LLC*. [http://dx.doi.org/10.1063/1.4870998]

Multifrequency atomic force microscopy (AFM) is an emerging[1,2] branch of AFM where two or more frequencies[3,4] are externally excited in order to map material composition,[5–7] enhance resolution[8] and sensitivity,[9–11] and quantify material properties[12–14] with gentle forces. The theory that controls the response of the cantilever while simultaneously exciting several frequencies and modes however is still emerging[12,15,16] and might result complex.[17,18] Here, possible mechanisms responsible for multiple regimes of operation in multifrequency AFM are discussed from the point of view of energy transfer in the presence of conservative and dissipative interactions. This is in line with recent reports discussing that multiple operation regimes can emerge in multifrequency AFM.[17–19] We report and discuss from a theoretical point of view and via numerical simulations that phase contrast arises from an interplay between energy dissipation and the kinetic energy, and energy transfer associated with the externally excited frequencies and eigenmodes.

The M equations of motion[20] that account for M cantilever modes can be written in the following way:[1]

$$\frac{k_{(m)}}{\omega_{(m)}^2}\ddot{z}_{(m)}(t)+\frac{k_{(m)}}{Q_{(m)}\omega_{(m)}}\dot{z}_{(m)}(t)+k_{(m)}z_{(m)}=F_D+F_{ts}, \quad (1)$$

where the subscript in brackets indicates mode m throughout. Then $k_{(m)}$, $Q_{(m)}$, $\omega_{(m)}$, and $z_{(m)}$ are the spring constant, quality factor, natural frequency, and position of the m eigenmode. F_D is the term standing for the external driving forces. Two external forces with magnitudes $F_{0(1)}$ and $F_{0(2)}$ and acting near $\omega_{(1)}$ and $\omega_{(2)}$ have been added here as in standard bimodal AFM.[1] The dynamics of the modes are coupled via the non-linear tip-sample force F_{ts}. The absolute position z is the sum of the M modes taken into account in the modal approximation

$$z\approx\sum_{m>0}^{M}z_{(m)} \quad (2)$$

or frequencies z_n

$$z\approx z_0+\sum_{n>0}^{N}z_n=z_0+\sum_{n>0}^{N}A_n\sin(n\omega t+\phi_n), \quad (3)$$

where the subscript without brackets stands for harmonic number n, z_0 is the mean deflection, and A_n and ϕ_n are the harmonic amplitudes and phases. The approximation implies that N is finite. Furthermore, the modes can also be decomposed into harmonic components

$$z_{(m)}\approx z_{(m)0}+\sum_{n>0}^{N}A_{(m)n}\sin(n\omega t+\phi_{(m)n}), \quad (4)$$

where, $z_{(m)0}$ is the mean deflection of mode m; suffixes for mode m and harmonic number n are employed as (m)n for amplitudes $A_{(m)n}$ and phases $\phi_{(m)n}$. Then, the net energy entering ($E_{T(m)}<0$) or leaving ($E_{T(m)}>0$) a given cantilever mode m can be written as

$$E_{T(m)}=-\oint F_{ts}.z_m dt, \quad (5)$$

where $\dot{z}_{(m)}$ is the time derivative of $z_{(m)}$ and $E_{T(m)}$ stands for net energy transfer (other than that lost to the viscous medium) per cycle via mode m. One can refer to such expression as Energy Transfer. In this work, two mechanisms accounting for $E_{T(m)}$ are identified, namely, (1) energy irreversibly lost in the tip-sample junction from mode m and (2) energy transfer from mode m to any other modes. The first mechanism requires the presence of dissipative forces while the second does not. Another key definition in dynamic AFM is that of the tip-sample virial

$$V_{(m)}=\frac{1}{T}\oint F_{ts}z_{(m)}dt, \quad (6)$$

where $V_{(m)}$ stands for tip-sample virial of mode m and T is the fundamental period. In general, $V_{(m)}$ might be positive or negative. For simplicity modes 1 and 2, i.e., m = 1 and m = 2, are accounted for in this work as in standard bimodal AFM.[1] A more common[21,22] definition of (5) and (6)

 © 2014 AIP Publishing LLC

This article is copyrighted as indicated in the article. Reuse of AIP content is subject to the terms at: http://scitation.aip.org/termsconditions. Downloaded to IP: 147.83.121.58 On: Fri, 06 Jun 2014 14:56:29

involves the harmonic terms only that coincide with, or lie near the, modal frequencies

$$E_{T(m)n} = -\oint F_{ts} A_{(m)n} n\omega \cos(n\omega t + \phi_{(m)n}) dt \approx E_{Tn} = \frac{n\pi k_{(m)} A_{0n} A_n}{Q_{(m)}} \left[\sin\phi_n - \frac{A_n}{A_{0n}}\right], \quad (7)$$

where m can take the values 1 and 2 and the corresponding harmonic numbers n are 1 and 6, respectively, and throughout. Furthermore, A_{0n} are the free amplitudes at ω ($n=1$) and 6ω ($n=6$) and it is assumed for simplicity that $\omega_{(1)} \approx \omega$ and $\omega_{(2)} \approx 6\omega$. Similarly[22]

$$V_{(m)n} = \frac{1}{T}\oint F_{ts} A_{(m)n} \sin(n\omega t + \phi_{(m)n}) dt \approx V_n = -\frac{1}{2}\frac{k_{(m)} A_{0n} A_n}{Q_{(m)}} \cos\phi_n. \quad (8)$$

Next we define the energy terms E_n for harmonics $n=1$ ($m=1$) and $n=6$ ($m=2$), respectively, as follows:

$$E_n = KE_n + E^*_{Tn}, \quad (9)$$

where KE_n stands for kinetic energy and it is computed as the energy associated with the nth harmonic as

$$KE_n = \frac{1}{2} k_{(m)} A_n^2. \quad (10)$$

Furthermore, E^*_{Tn} is related to E_{Tn} in (7) by

$$E^*_{Tn} = \frac{E_{Tn} Q_{(m)}}{2\pi n}. \quad (11)$$

Combining these expressions leads to the phase shifts of harmonics 1 and 6 (monitored in bimodal AFM) in terms of the inverse tangent and inverse cosine functions

$$\phi_n \approx \tan^{-1}\left[\frac{-E_n}{V_n Q_{(m)}}\right] \approx \cos^{-1}\left[\frac{-2V_n Q_{(m)}}{k_{(m)} A_{0n} A_n}\right]. \quad (12)$$

This expression is equivalent to those derived by others[23,24] but its interpretation here leads to key results relating to energy transfer and phase contrast as discussed below. In standard AM AFM the fundamental phase shift ϕ_1 might lie above or below 90° in what defines two distinct force regimes,[25] i.e., the attractive and the repulsive regimes, where the average tip-sample force F_{AV} is attractive or repulsive, respectively. From now on, the average force F_{AV} being negative or positive will be employed to define attractive and repulsive force regimes, respectively. The inverse tangent relationship in (12), however, suggest 4 possible combinations or regimes of operation at both harmonics $n=1$ ($m=1$) and $n=6$ ($m=2$), respectively. This follows from the fact that both V_n in (8) and E_n in (9) can, in principle, be positive or negative. A closer look at (12), however, indicates that the sign of the virial alone controls whether the phase lies above or below 90° since the inverse cosine relationship depends on V_n only. Then it also follows from the inverse tangent relationship in (12) that it is a necessary condition that $E_1 > 0$ ($m=1$) and that $E_6 > 0$ ($m=2$). This is a main hypothesis in this work, and has some important implications:

(1) First, E^*_{T1} (and E^*_{T6}) might be negative or positive implying that during the tip-sample interaction energy transfer might be positive or negative at $n=1$ and/or $n=6$. This is consistent for both conservative and dissipative interactions since no assumptions have been made in terms of the character of the forces. Also note that in monomodal AFM it is required that $E^*_{Tn} < 0$ for $n > 1$.
(2) Second, it necessarily follows from (12) that $KE_1 > -E^*_{T1}$ ($E_1 > 0$) and that $KE_6 > -E^*_{T6}$ ($E_6 > 0$).
(3) Third, for conservative interactions it is a necessary condition that $E_{T(1)} = -E_{T(2)}$ or, in terms of the monitored frequencies, $E_{T1} \approx -E_{T6}$.

The third point follows directly from the energy conservation principle. Note that the energy dissipated per cycle E_{dis} can be written as

$$E_{dis} = E_{T(1)} + E_{T(2)}. \quad (13)$$

Then, for a conservative system where $E_{dis} = 0$ it follows that $E_{T(1)} = -E_{T(2)}$. For a more general system, where other eigenmodes are included ($M > 2$) energy transfers between the M modes when $E_{dis} = 0$. The energy transfer between modes 1 and 2 is illustrated in Fig. 1.

The expressions above are next compared to the results of numerical integration. In the long range F_{ts} is defined by the Hamaker constant H, the tip radius R, and the tip sample distance d[22]

$$F_{ts}(d) = -\frac{RH}{6d^2} \quad a_0 < d, \quad (14)$$

where a_0 (≈ 0.165 nm) is an intermolecular distance. The distance d and the tip position z are related via the cantilever separation z_c since $d = z_c + z$.

For Fig. 2, the parameters are: $A_{01} = 5$ nm, $A_1 = 4$ nm, $k_{(1)} = 2$ N/m, $k_{(2)} = 80$ N/m, $Q_{(1)} = 100$, $Q_{(2)} = 600$, $f_{(1)} = 70$ kHz ($\omega_{(1)} = 2\pi f_{(1)}$), $f_{(2)} = 42$ kHz ($\omega_{(2)} = 2\pi f_{(2)}$), $H = 4.1 \times 10^{-19}$ J and $R = 5$ nm. Only the second mode phenomena corresponding with harmonic 6 are discussed in detail for

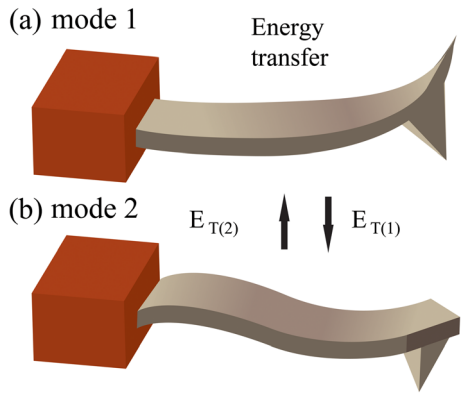

FIG. 1. Illustration of how energy might transfer between modes (a) 1 and (b) 2.

This article is copyrighted as indicated in the article. Reuse of AIP content is subject to the terms at: http://scitation.aip.org/termsconditions. Downloaded to IP: 147.83.121.58 On: Fri, 06 Jun 2014 14:56:29

simplicity and because the corresponding channels A_6 and ϕ_6 provide[1] compositional contrast. With these parameters d always lied above a_0 ($d > a_0$) in the simulations. Thus, the example in Fig. 2 corresponds to bimodal AFM operated in the standard attractive regime where $F_{AV} < 0$. Note also that in Fig. 2, F_{ts} is conservative, i.e., $E_{dis} = 0$. In the figure, the free amplitude of the second mode (sixth harmonic) A_{06} has been varied in the range 0.1–5 nm since this is characteristic of standard values in bimodal AFM.[1,14,15] Fig. 2(a) shows variations of KE_6 (squares) and E^*_{T6} (circles) with A_{06}. The energies have been normalized with 6.2 keV. KE_6 monotonously increases with A_{06}, whereas $E^*_{T6} < 0$ throughout. The numerical values are $E^*_{T6} = -0.3$, -1.7154, -2.5318, -2.9002, -3.0365, and -3.1318 eV for $A_{06} = 0.1$, 1, 2, 3, 4, and 5 nm, respectively. By comparing these results with $KE_6 = 3.1$, 239.2, 972.3, 2211.6, 3954.1, and 6198.1, it follows that the condition $KE_6 > -E^*_{T6}$ is satisfied. The normalized values of E_6 (rhombuses) and V_6 (crosses) are plotted in Fig. 2(b); $E_6 > 0$ and $V_6 > 0$ throughout with maxima of 6.2 keV and 0.9 eV, respectively. In terms of the observable ϕ_6 this implies that $\phi_6 > 90°$ throughout (Fig. 2(c)) in accordance with the prediction of (12). According to the simulations here, these results should be standard in bimodal AFM in the attractive regime where $F_{AV} < 0$. That is, $\phi_6 > 90°$ independently of A_{06}. Furthermore, from the numerical results it was also verified that $E_{T1} \approx -E_{T6}$, and, more thoroughly, $E_{T(1)} = -E_{T(2)}$ exactly. In summary, in the attractive regime the three conditions above are satisfied according to the simulations here.

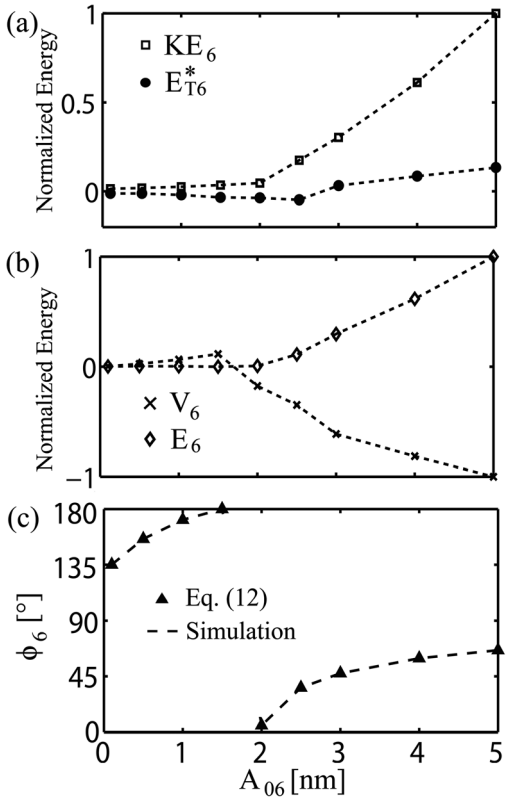

FIG. 3. Response (conservative forces only) of experimental observables and expressions that can be computed from observables in bimodal AFM in the repulsive regime as a function of second mode (sixth harmonic) free amplitude A_{06}.

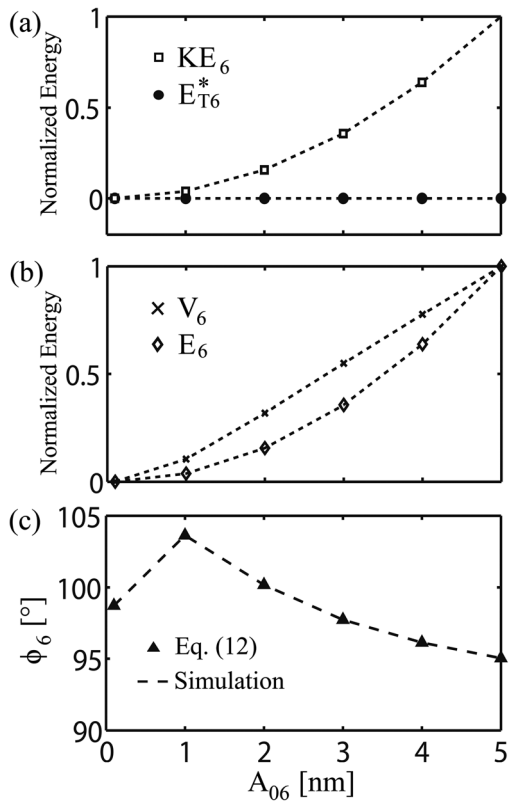

FIG. 2. Results of the experimental observables and expressions that can be computed from observables in bimodal AFM in the attractive regime as a function of second mode (sixth harmonic) free amplitude A_{06}.

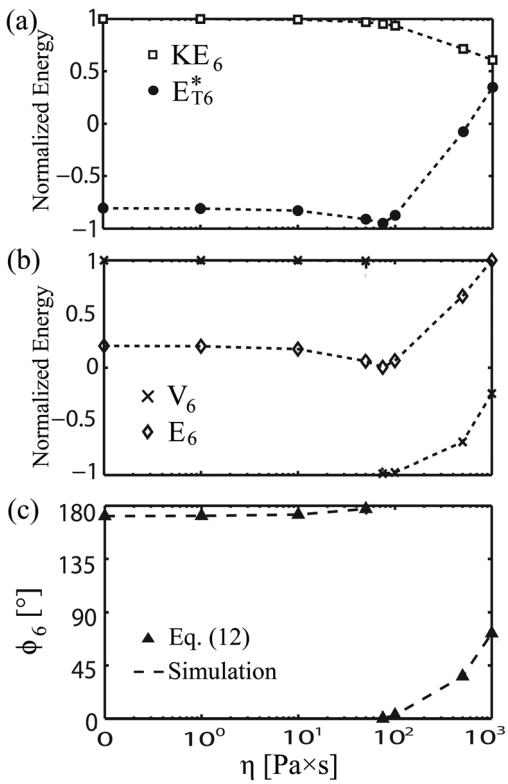

FIG. 4. Response (conservative and dissipative forces) of experimental observables and expressions that can be computed from observables in bimodal AFM in the repulsive regime as a function of viscosity η.

This article is copyrighted as indicated in the article. Reuse of AIP content is subject to the terms at: http://scitation.aip.org/termsconditions. Downloaded to IP: 147.83.121.58 On: Fri, 06 Jun 2014 14:56:29

TABLE I. Numerical values corresponding to the results in Fig. 3. The number of the equation employed is written in brackets in the first column.

A_{06} [nm]	0.1	0.5	1	1.5	2	2.5	3	4	5
$E_{T(1)}$ [eV] (5)	5.93	8.86	11.29	12.82	13.88	17.78	19.03	20.1	20.51
$E_{T(2)}$ [eV] (5)	−5.93	−8.86	−11.29	−12.82	−13.88	−17.78	−19.03	−20.1	−20.51
$V_{(1)}$ [eV] (6)	−10.18	−9.84	−9.53	−9.33	−9.18	−8.59	−8.39	−8.22	−8.16
$V_{(2)}$ [eV] (6)	−0.01	−0.12	−0.31	−0.56	−0.86	−1.7	−2.24	−3.17	−4.05
V_6 [eV] (8)	0.02	0.12	0.32	0.56	−0.86	−1.71	−3.00	−3.99	−4.89
E_6 [eV] (9)	10.22	33.45	29.22	0.43	49.01	739.69	1960.97	4079.16	6632.22
KE_6 [eV] (10)	83.89	107.22	150.24	203.35	269.69	1022.68	1773.73	3583.63	5853.96
E^*_{T6} [eV] (11)	−73.67	−73.77	−121.01	−202.92	−220.68	−282.99	187.25	495.53	778.25
ϕ_1 [°] (12)	35.11	37.76	40.03	41.49	42.51	46.45	47.74	48.85	49.24
ϕ_6 [°] (12)	135.05	155.86	171.32	179.93	5.42	35.85	47.46	59.61	66.13
$E_{(2)6}$ [eV] (17)	−10.52	−33.73	−29.48	−0.64	48.85	739.73	1470.91	3263.71	5527.47
δ [nm]	1.07	1.15	1.23	1.3	1.37	1.57	1.66	1.79	1.88
F_{AV} [pN]	86.67	84.18	82.38	81.63	81.46	76.79	74.91	73.04	72.19

Next, bimodal AFM is operated in the repulsive regime where $F_{AV} > 0$. For this purpose, a repulsive force[22,25] is employed when $a_0 \leq d$

$$F_{ts}(d) = -\frac{RH}{6a_0^2} + \frac{4}{3}E^*\sqrt{R}\delta^{3/2} \quad a_0 \geq d\,, \tag{15}$$

where d and the tip-sample deformation δ are related by $\delta = a_0 - d$. E^* (≈1 GPa in this work) is the effective Young's modulus in the contact and A_{06} has been varied from 0.1 to 5 nm. The results are shown in Fig. 3 for: $A_{01} = 10$ nm, $A_1 = 10$ nm, and $H = 2.1 \times 10^{-20}$ J (all other parameters as in Fig. 2). The first thing to note from Fig. 3(a) is that E^*_{T6} (circles) goes from negative to positive for $A_{06} = 2.5$–3 nm. Physically this implies that for small values A_{06} or KE_6 the energy transferred to $n = 6$ are positive. However, when KE_6 (squares) is sufficiently large (∼1 keV in Fig. 3(a)) energy transfers from the 6th frequency (mode 2) to other frequencies. The numerical values are provided in Table I. Again Figs. 3(b) and 3(c) confirm that $E_6 > 0$ and that V_6 alone controls whether ϕ_6 lies above or below 90°. In particular, V_6 becomes negative in Fig. 3(b) for $A_{06} = 1.5$–2 nm and the phase transition follows (Fig. 3(c)). Numerical values of the corresponding δ and F_{AV} are also given in Table I (discussed below).

As another test to the theory above, a dissipative force can be added in the contact region[11,26]

$$F_{dis}(\delta) = -\eta(R\delta)^{1/2}\dot{\delta} \quad \delta > 0\,. \tag{16}$$

The range of values given to the viscous coefficient η in Fig. 4 is; $\eta = 0$, 1, 10, 75, 100, 500, and 1000 Pa s (x-axis). The rest of parameters are as in Fig. 3 except for A_{06} which is 1 nm throughout. Fig. 4(a) shows that KE_6 (squares) decreases with increasing η and dissipation (E_{dis}). The energy transfer E^*_{T6} (circles) goes from negative to positive with increasing η. Again $E_6 > 0$ (Fig. 4(b) rhombuses) throughout (see Table II) and the sign of V_6 (crosses) alone defines whether ϕ_6 lies above or below 90° (Fig. 4(c)).

Finally, we note an interesting physical observation. Namely, even if $V_6 > 0$, and provided $F_{AV} > 0$, the mode virial in (6) gives $V_{(m)} < 0$. This implies that ϕ_6 does not follow from the sign of $V_{(m)}$; see the corresponding numerical values in Table II and compare $V_{(m)}$, F_{AV}, ϕ_1, and ϕ_6. F_{AV} is also shown in Table I for the results in Fig. 3 where it can be seen that F_{AV} decreases monotonously with increasing A_{06}.

TABLE II. Numerical values corresponding to the results in Fig. 4. The number of the equation employed is written in brackets in the first column.

η [Pa s]	0	1	10	50	75	100	500	1000
$E_{T(1)}$ [eV] (5)	11.29	11.32	11.52	12.41	12.94	13.45	19.88	26.31
$E_{T(2)}$ [eV] (5)	−11.29	−11.26	−10.97	−9.71	−8.97	−8.25	−0.74	3.28
$V_{(1)}$ [eV] (6)	−9.53	−9.53	−9.50	−9.38	−9.31	−9.24	−8.22	−6.92
$V_{(2)}$ [eV] (6)	−0.31	−0.31	−0.31	−0.31	−0.31	−0.31	−0.22	−0.09
V_6 [eV] (8)	0.32	0.32	0.32	0.32	−0.31	−0.31	−0.22	−0.08
E_6 [eV] (9)	29.22	28.80	24.97	8.82	0.54	9.33	95.61	143.64
KE_6 [eV] (10)	150.23	150.15	149.35	145.55	143.02	140.43	107.23	91.263
E^*_{T6} [eV] (11)	−121.01	−121.35	−124.39	−136.74	−142.49	−131.10	−11.63	52.38
ϕ_1 [°] (12)	40.03	40.06	40.26	41.11	41.63	42.12	48.83	56.62
ϕ_6 [°] (12)	171.32	171.45	172.57	177.35	0.16	2.86	35.76	72.13
$E_{(2)6}$ [eV] (17)	−29.48	−29.05	−25.22	−9.06	0.30	9.10	95.40	143.42
δ [nm]	1.23	1.23	1.23	1.22	1.21	1.20	1.05	0.89
F_{AV} [pN]	82.38	82.36	82.14	81.18	80.60	80.02	71.40	59.35
E_{dis} [eV] (13)	0.00	0.06	0.56	2.70	3.97	5.20	19.13	29.59

This article is copyrighted as indicated in the article. Reuse of AIP content is subject to the terms at: http://scitation.aip.org/termsconditions. Downloaded to IP: 147.83.121.58 On: Fri, 06 Jun 2014 14:56:29

This however does not imply that the interaction becomes gentle by increasing the amplitude of the second mode in bimodal AFM. On the contrary, the tip-sample deformation δ increases monotonously with increasing A_{06} (Table I). As dissipation increases however, and for a given A_{06}, δ decreases monotonously with increasing η and E_{dis} (Table II) as in standard AFM.[27–29] Let us, however, define a modal energy term $E_{(m)}$ similar to that of the frequency term in (9)

$$E_{(m)n} = KE_n + \frac{E_{T(m)}Q_{(m)}}{2\pi n}. \tag{17}$$

The numerical values of (17) are shown in Tables I and II for mode $m = 2$ and harmonic $n = 6$. The sign of $E_{(2)6}$ is now observed to follow the transitions of ϕ_6 as opposed to the sign of the modal virial $V_{(2)}$ and the average force F_{AV}.

In summary, phase contrast in bimodal AFM has been discussed in terms of energy transfer between modes, energy dissipation and the kinetic energy, and energy transfer associated with the harmonic component externally driven at mode 2 and close to resonance, here harmonic 6. In the simulations here and in the attractive regime where the average force is negative, the single frequency virial remained positive for the two monitored frequencies and the corresponding phase shifts lied above 90° throughout. On the other hand, in the repulsive regime the single frequency virial, and the corresponding phase shift, might undergo transitions in sign as reported by some.[18,19] Such transitions might occur even when the average force and the modal virial remain negative. The results should be general for any higher eigenmodes since no assumptions have been made in terms of higher mode number.

The artistic figure was designed by Maritsa Kissamitaki.

[1]T. Rodriguez and R. Garcia, Appl. Phys. Lett. **84**(3), 449–551 (2004).
[2]R. Garcia and E. T. Herruzo, Nat. Nanotechnol. **7**, 217–226 (2012).
[3]S. D. Solares and G. Chawla, J. Appl. Phys. **108**, 054901 (2010).
[4]S. D. Solares and G. Chawla, Meas. Sci. Technol. **21**, 125502 (2010).
[5]R. Garcia and R. Proksch, Eur. Polym. J. **49**(8), 1897–1906 (2013).
[6]R. Proksch, Appl. Phys. Lett. **89**, 113121 (2006).
[7]G. Chawla and S. D. Solares, Appl. Phys. Lett. **99**, 074103 (2011).
[8]S. Kawai, T. Glatzel, S. Koch, B. Such, A. Baratoff, and E. Meyer, Phys. Rev. Lett. **103**, 220801 (2009).
[9]S. Kawai, T. Glatzel, S. Koch, B. Such, A. Baratoff, and E. Meyer, Phys. Rev. B **81**, 085420 (2010).
[10]S. Patil, N. F. Martinez, J. R. Lozano, and R. Garcia, J. Mol. Recognit. **20**, 516–523 (2007).
[11]S. Santos, Appl. Phys. Lett. **103**, 231603 (2013).
[12]E. T. Herruzo, A. P. Perrino, and R. Garcia, Nat. Commun. **5**, 3126 (2014).
[13]D. Forchheimer, D. Platz, E. A. Tholén, and D. B. Haviland, Phys. Rev. B **85**, 195449 (2012).
[14]D. Martinez-Martin, E. T. Herruzo, C. Dietz, J. Gomez-Herrero, and R. Garcia, Phys. Rev. Lett. **106**, 198101 (2011).
[15]M. D. Aksoy and A. Atalar, Phys. Rev. B **83**, 075416 (2011).
[16]E. T. Herruzo and R. Garcia, Beilstein J. Nanotechnol. **3**, 198–206 (2012).
[17]R. Stark, Appl. Phys. Lett. **94**, 063109 (2009).
[18]D. Kiracofe, A. Raman, and D. Yablon, Beilstein J. Nanotechnol. **4**, 385–393 (2013).
[19]I. Chakraborty and D. G. Yablon, Nanotechnology **24**(47), 475706 (2013).
[20]R. Steidel, *An Introduction to Mechanical Vibrations*, 3rd ed. (John Wiley & Sons, 1989).
[21]J. P. Cleveland, B. Anczykowski, A. E. Schmid, and V. B. Elings, Appl. Phys. Lett. **72**(20), 2613–2615 (1998).
[22]A. S. Paulo and R. Garcia, Phys. Rev. B **64**, 193411 (2001).
[23]J. R. Lozano and R. Garcia, Phys. Rev. Lett. **100**, 076102 (2008).
[24]J. R. Lozano and R. Garcia, Phys. Rev. B **79**, 014110 (2009).
[25]R. Garcia and A. San Paulo, Phys. Rev. B **60**(7), 4961–4967 (1999).
[26]A. F. Payam, J. R. Ramos, and R. Garcia, ACS Nano **6**(6), 4663–4670 (2012).
[27]S. Santos, K. R. Gadelrab, T. Souier, M. Stefancich, and M. Chiesa, Nanoscale **4**, 792–800 (2012).
[28]R. Garcia, C. J. Gómez, N. F. Martinez, S. Patil, C. Dietz, and R. Magerle, Phys. Rev. Lett. **97**, 016103 (2006).
[29]H. V. Guzman, A. P. Perrino, and R. Garcia, ACS Nano **7**(4), 3198–3204 (2013).

This article is copyrighted as indicated in the article. Reuse of AIP content is subject to the terms at: http://scitation.aip.org/termsconditions. Downloaded to IP: 147.83.121.58 On: Fri, 06 Jun 2014 14:56:29